PHYSICAL REVIEW D **81,** 094022 (2010)

Quark propagator in the Nambu–Jona-Lasinio model in a self-consistent $1/N_c$ expansion

D. Müller, M. Buballa, and J. Wambach
Institut für Kernphysik, Technische Universität Darmstadt, Germany
(Received 8 March 2010; published 20 May 2010)

The quark propagator is calculated in the Nambu–Jona-Lasinio model in a self-consistent $1/N_c$-expansion at next-to-leading order. The calculations are carried out iteratively in Euclidean space. The chiral quark condensate and its dependence on temperature and chemical potential is calculated directly and compared with the mean-field results. In the chiral limit, we find a second-order phase transition at finite temperature and zero chemical potential, in agreement with universality arguments. At zero temperature and finite chemical potential, the phase transition is first order. In comparison with the mean-field results, the critical temperature and chemical potential are slightly reduced. We determine spectral functions from the Euclidean propagators by employing the maximum-entropy method. Thereby quark and meson masses are estimated and decay channels identified. For testing this method, we also apply it to evaluate perturbative spectral functions, which can be calculated directly in Minkowski space. In most cases we find that the maximum-entropy method is able to reproduce the rough features of the spectral functions, but not the details.

DOI: 10.1103/PhysRevD.81.094022 PACS numbers: 12.39.Fe, 11.15.Pg, 11.30.Rd

I. INTRODUCTION

Describing the low-energy sector of QCD is a complicated task due to its strong coupling. Especially investigating the region of the chiral and deconfinement phase transition requires nonperturbative methods. To describe these phenomena, one therefore often employs effective models, which give a simplified description of the theory and are valid in a limited energy range. In this article, we focus on the Nambu–Jona-Lasinio (NJL) model [1], where the quark-gluon interactions of QCD are substituted by effective four-quark interactions. This model does not exhibit confinement, which is its major lack, but it incorporates chiral symmetry. Spontaneous and explicit breaking of this symmetry as well as its restoration at high temperatures or densities can be realized.

Despite the simplifications in the interaction, the NJL model cannot be solved exactly, but further approximations are necessary.[1] In most publications, the model has been treated in mean-field (Hartree) and random-phase approximation to describe the chiral dynamics of quarks and the meson spectrum, both in vacuum and in hot and dense matter [3–5]. A shortcoming of these approximations is that the effects of mesons on the quark propagator are not included. In the quark sector this leads to the wrong universal behavior at the phase transition and produces delta peaked quark spectral functions. As a consequence, for instance, they are not suitable to be used in the Kubo formula for the calculation of shear viscosities [6]. In the mesonic sector, hadronic decay channels, like $\rho \to \pi\pi$, are not included, which are the physical decay channels in the confined phase.

These processes can be included systematically within a $1/N_c$ expansion, i.e., within an expansion in the inverse number of colors, beyond the leading order; see, e.g., Refs. [7–16]. Here one can basically follow two different approaches: In the ''strict $1/N_c$ expansion scheme'' one first solves the gap equation in leading order, i.e., Hartree approximation, and then adds the $1/N_c$ corrections to the quantities of interest perturbatively, without modifying and solving the gap equation again. This method yields good results, e.g., for the rho meson dominated electromagnetic pion form factor in the timelike region [14] as well as for the low-temperature behavior of the quark condensate [11,15] and the pressure [16]. Above the critical temperature the model has been studied in [17] where the influence of soft modes on the quark spectral function was investigated. On the other hand, the perturbative approach breaks down in the vicinity of the phase transition, where a method is needed which incorporates the $1/N_c$ corrections self-consistently in the gap equation. First attempts in this direction have been performed in Refs. [9,13,15], but in a simplified approach, where nonlocal contributions to the quark self-energy have been neglected. This scheme is thermodynamically inconsistent and it was found that the chiral phase transition at finite temperature is first order for two quark flavors [13,15], in contradiction to universality arguments [18].

In the present paper, we derive a self-consistent solution of the gap equation using the so-called Φ-derivable theory in next-to-leading order without further approximations. This approach is thermodynamically consistent and allows a meaningful investigation of the phase transition. Because

[1]Strictly speaking, since the NJL model is nonrenormalizable, a unique exact solution does not even exist, but the results depend on the regularization scheme. An interesting alternative to the continuum methods discussed in this article is to solve the NJL model on the lattice [2]. In this case the nonrenormalizability has the consequence that there is no continuum limit, so that the results depend on the choice of the lattice.

of the nonlocal self-energy contributions, the structure of the equations is rather involved and we use the imaginary time (Matsubara) formalism to keep them on a tractable level. This allows us to study static properties, like the quark condensate at zero and finite temperature. On the other hand, the analytic continuation of dynamical quantities to real times is problematic. In order to gain information about quark and meson spectral functions in Minkowski space, we therefore employ the maximum-entropy method (MEM).

The remainder of this article is organized as follows. In Sec. II we summarize the basics of the model and the leading-order formalism. In Sec. III we introduce the Φ-derivable theory and formally derive the gap equation for the quark propagator in next-to-leading order (NLO) in $1/N_c$. The numerical results for the self-consistent solutions in the Matsubara formalism are shown in Sec. IV. There, we also discuss the behavior of the quark condensate as a function of temperature and chemical potential. In Sec. V we review the basic ideas of MEM and apply them to study quark and meson spectral functions. We conclude with a summary in Sec. VI.

II. MODEL AND LEADING ORDER FORMALISM

We use a two-flavor NJL model with a scalar and pseudoscalar interaction, given by the Lagrangian

$$\mathcal{L} = \bar{q}(i\not{\partial} - m_0)q + G[(\bar{q}q)^2 + (\bar{q}i\gamma_5\vec{\tau}q)^2] \quad (1)$$

with a dimensionful coupling constant G and the Pauli matrices $\vec{\tau}$ in isospin space. m_0 is a small bare quark mass, which explicitly breaks chiral symmetry. For calculations in the chiral limit, it is set to zero. In this limit the Lagrangian is invariant under $SU(2)_L \times SU(2)_R$ transformations. For nonvanishing but small values of m_0, this is still an approximate symmetry of the model.

The $1/N_c$ counting scheme is introduced in the NJL model by assuming that the quark fields q have N_c color degrees of freedom. Consequently, a closed quark loop yields a factor N_c. Furthermore, it is assumed that the coupling constant G scales like $1/N_c$. In this article these rules are used to organize the diagrams in a systematic and symmetry conserving way. In all explicit calculations, however, we take the physical number of colors, $N_c = 3$.

In any approximation the full quark propagator $S(k)$ is given by

$$S^{-1}(k) = S_0^{-1}(k) - \Sigma(k) \quad (2)$$

with the inverse bare propagator $S_0^{-1}(k) = \not{k} - m_0$ and a self-energy $\Sigma(k)$. For large enough couplings, chiral symmetry is spontaneously broken and the quarks acquire a dynamical mass much larger than the bare mass. In leading order in $1/N_c$ this is described by the Hartree Dyson equation, Fig. 1. In the self-energy insertion on the right-hand side (r.h.s.), the factor N_c of the quark loop is compensated by a factor $1/N_c$ from the vertex. Hence, if we assume that the bare propagator is of the order N_c^0, we find that the dressed propagator in Hartree approximation is strictly of the order N_c^0 as well. Note that in this paper we draw the local four-point interaction as a wavy line, indicating the direction of the interaction. In the present example this prevents confusion of the Hartree term with the Fock term, which is suppressed by one order of $1/N_c$.

FIG. 1. Dyson-equation for the Hartree quark propagator (bold lines). Thin lines represent the bare propagator, the wavy line the bare interaction.

In vacuum, the Hartree self-energy is given by

$$\Sigma_H = 2iG \int \frac{d^4k}{(2\pi)^4} \mathrm{Tr}(S(k)). \quad (3)$$

It is local and purely scalar and therefore corresponds to a constant shift in the quark mass,

$$m_H = m_0 + \Sigma_H. \quad (4)$$

The dressed or ''constituent quark'' mass m_H is the scalar part of the inverse Hartree propagator $S^{-1}(k) = \not{k} - m_H$. In this way it enters the r.h.s. of Eq. (3), thereby giving rise to a self-consistency problem.

To describe the system at nonvanishing temperature T and chemical potential μ, we apply the Matsubara formalism. The quark propagator is then defined at discrete imaginary energies $i\omega_n + \mu$, with fermionic Matsubara frequencies $\omega_n = (2n+1)\pi T$. Accordingly, the energy integration in fermionic loop integrals is replaced by a sum,

$$i\int \frac{d^4k}{(2\pi)^4} f(k_0, \vec{k}) \to -T\sum_n \int \frac{d^3k}{(2\pi)^3} f(i\omega_n + \mu, \vec{k}). \quad (5)$$

In the Hartree approximation, where the self-energy is just a constant, the analytic continuation of the propagator to real energies is, of course, trivial. However, this will no longer be the case at NLO.

Mesons are described by a Bethe-Salpeter equation (BSE) for the quark-antiquark T matrix,

$$i\hat{T}(q) = i\hat{K} + i\hat{K}(-i\hat{\Pi}(q))i\hat{T}(q). \quad (6)$$

The leading order corresponds to the random-phase approximation (RPA), depicted in Fig. 2. In this case

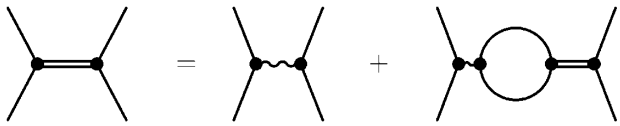

FIG. 2. Bethe-Salpeter equation for quark-antiquark scattering. Double lines denote RPA meson propagators.

$$i\hat{K} = 2iG\sum_M (\Gamma_M \otimes \Gamma_M) \tag{7}$$

is the bare scattering kernel and

$$J_M(q) \equiv \Gamma_M \hat{\Pi}(q)\Gamma_M = i\int \frac{d^4k}{(2\pi)^4}\,\mathrm{Tr}[\Gamma_M S(k+q)\Gamma_M S(k)] \tag{8}$$

are the quark-antiquark polarization functions in the scalar and pseudoscalar channels,

$$\Gamma_s = \mathbb{1}, \qquad \Gamma_{p,a} = i\gamma_5\tau_a. \tag{9}$$

Here we have used the fact that these channels do not mix. Equation (6) is then easily solved with the ansatz

$$\hat{T}_M = -D_M(\Gamma_M \otimes \Gamma_M), \tag{10}$$

which yields

$$D_M(q) = \frac{-2G}{1-2GJ_M(q)}. \tag{11}$$

Following Refs. [14,15], we will call the functions $D_M(q)$ ''meson propagators'' although they are not properly normalized. In particular, the meson masses are given by the pole positions of the propagators,

$$D_M^{-1}(q)|_{q^2=m_M^2} = 0. \tag{12}$$

When we expand the r.h.s. of Fig. 2 into a geometric series, we see that the term with n quark loops contains $n+1$ four-point vertices. Thus, applying the $1/N_c$ counting rules, we find that the RPA meson propagators are strictly of the order $1/N_c$.

In the Matsubara formalism, the meson propagators and polarization functions are defined at discrete imaginary energies $i\omega_m$, with bosonic Matsubara frequencies $\omega_m = 2m\pi T$. The determination of meson masses according to Eq. (12) then requires the analytic continuation of the propagator to real energies. Again, this is easily done in the Hartree + RPA scheme, but will be nontrivial at NLO.

III. Φ-DERIVABLE THEORY

As motivated in the introduction we are aiming at a self-consistent extension of the approximation scheme beyond the leading order in $1/N_c$. To this end we apply the $1/N_c$ expansion on the level of the thermodynamic potential using the so-called Φ-derivable theory [19,20]. This scheme preserves all important symmetries.

The full thermodynamic potential is given by

$$\Omega[S] = i\,\mathbf{Tr}\ln S^{-1} + i\,\mathbf{Tr}(\Sigma S) + \Phi[S], \tag{13}$$

where S and $\Sigma = S_0^{-1} - S^{-1}$ are the full quark propagator and the full self-energy, respectively, and **Tr** denotes a functional trace over all space-time and internal degrees of freedom. The functional $\Phi[S]$ summarizes all closed two-particle irreducible diagrams [21].

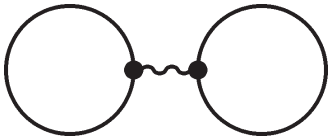

FIG. 3. Leading order contribution to Φ.

The stationarity condition $\frac{\delta\Omega}{\delta(iS)} = 0$ implies that

$$\Sigma(x) = -\frac{\delta\Phi}{\delta(iS(x))}, \tag{14}$$

i.e., the self-energy can be obtained as a functional derivative of Φ. Diagrammatically, this corresponds to cutting a single quark line of Φ at all possible places. In turn, Φ depends on Σ via the full quark propagator. Equation (14) therefore constitutes a self-consistency problem.

Similarly, the symmetry conserving scattering kernel for the mesonic BSE can be obtained as

$$\hat{K}(x,y) = -\frac{\delta^2\Phi}{\delta(iS(x))\delta(iS(y))}, \tag{15}$$

corresponding to cutting the Φ functional twice. However, unlike for the self-energy, this is not a self-consistency problem because Φ does not depend on $\hat{K}$.

Self-consistent approximation schemes can now be introduced by performing truncations of the functional Φ. In the present article, we expand Φ in powers of $1/N_c$ to next-to-leading order. The leading-order contribution corresponds to the ''glasses'' diagram, shown in Fig. 3. In vacuum it is given by

$$\Phi^{(0)}[S] = -G\sum_M\left(-i\int\frac{d^4k}{(2\pi)^4}\,\mathrm{Tr}(\Gamma_M S(k))\right)^2, \tag{16}$$

which can be generalized in the Matsubara formalism by the replacement (5). As it contains two quark loops and one four-point vertex, it is of the order $\mathcal{O}(N_c)$. Cutting one or two quark lines, we reproduce our earlier result that the Hartree self-energy and the RPA scattering kernel, respectively, are the corresponding leading-order expressions in this expansion. Formally, this can also be obtained from Eqs. (14) and (15), where one has to take into account that the transformation to momentum space brings in extra factors of $(2\pi)^4$. For instance, for the self-energy one gets

$$\Sigma(k) = i(2\pi)^4\frac{\delta\Phi}{\delta S(k)}, \tag{17}$$

which, when applied to Eq. (16), indeed yields Eq. (3).

The fact that the Hartree self-energy and the RPA scattering kernel can consistently be derived from the same Φ-functional guarantees that this approximation scheme is symmetry conserving. In particular, chiral Ward identities and low-energy theorems are fulfilled and the RPA pion is massless in the chiral limit, as required by Goldstone's theorem.

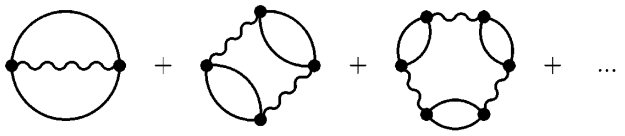

FIG. 4. NLO contribution to Φ.

The NLO correction to Φ is given by the ring sum, depicted in Fig. 4. Taking into account the appropriate symmetry factors, these diagrams can be combined to a logarithm. One obtains

$$\Phi^{(1)}[S] = -\frac{i}{2}\sum_M \int \frac{d^4q}{(2\pi)^4} \ln(1 - 2GJ_M(q)), \qquad (18)$$

which depends on S through the polarization function J_M, Eq. (8). Applying again Eq. (17), we find the following NLO correction to the self-energy:

$$\Sigma^{(1)}(k) = i\sum_M \int \frac{d^4q}{(2\pi)^4} D_M(q)\Gamma_M S(k-q)\Gamma_M. \qquad (19)$$

It describes the dressing of the quark propagator by an RPA meson and corresponds to the insertion in the last diagram in Fig. 5. Recalling that the RPA meson propagators are of the order $1/N_c$, this self-energy term yields a correction of the order $1/N_c$ to the quark propagator. However, when the diagrams are iterated in the gap equation, as shown in the figure, higher orders are generated. Therefore both, the self-consistent quark propagator and the individual self-energy contributions, are no longer of strict orders in $1/N_c$. Obviously, the same is true for $\Phi^{(0)}$ and $\Phi^{(1)}$ which contain higher orders in $1/N_c$ as well, when the self-consistent quark propagator is used. In the present scheme, the $1/N_c$ counting is thus introduced on the level of skeleton diagrams for the Φ functional, i.e., before dressing the propagators.

As we have discussed, at leading order RPA mesons together with the Hartree gap equation are consistent with chiral Ward identities so that, in the chiral limit, pions emerge as massless Goldstone bosons in that scheme. In the same way one can construct mesons which are consistent with the NLO gap equation. To that end one has to calculate the NLO corrections to the scattering kernel by applying Eq. (15) to $\Phi^{(1)}$, corresponding to cutting the diagrams in Fig. 4 twice, and iterate them together with the leading-order kernel in the BSE. Again, this scheme preserves chiral symmetry and the resulting pions are massless in the chiral limit.

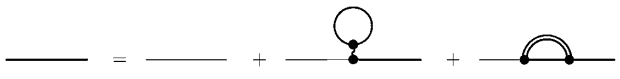

FIG. 5. NLO gap equation. The thin and bold lines represent bare and dressed quark propagators, respectively. The double line symbolizes RPA-like mesons as defined in Fig. 2 but involving the self-consistent solution for the quark propagator.

In this context it should be noted that the mesons which enter the NLO self-energy diagram are *not* the NLO-corrected mesons, but RPA mesons. To be precise, they are obtained from the BSE with the leading-order scattering kernel, Fig. 2, but the polarization functions J_M, Eq. (8), involve the self-consistent NLO quark propagators. As a consequence, these "intermediate mesons" are not restricted by chiral Ward identities and the pions are not necessarily massless in the chiral limit. Formally, this problem is a higher-order effect in $1/N_c$ but, as we will see below, it is quite severe. It can be avoided by performing a "strict $1/N_c$-expansion," where only the Hartree gap equation is solved self-consistently and the NLO corrections are added perturbatively, discarding all higher-order terms. Then all diagrams contain only Hartree quark propagators and, hence, the intermediate RPA pions are massless in the chiral limit. As shown, e.g., in Refs. [11,14–16] this perturbative treatment yields the correct results for the low-temperature behavior of the quark condensate and the pressure. However, since the focus of the present paper is on the phase transition, which cannot be treated perturbatively, we stay with the self-consistent expansion scheme outlined above. We should then be alerted to the fact that the intermediate RPA mesons do not obey the chiral Ward identities.

IV. NUMERICAL RESULTS

In this section we present numerical solutions of the self-consistent gap equation at NLO and related quantities. The main complication as compared to the leading-order problem arises from the fact that the NLO self-energy correction (last diagram in Fig. 5) is nonlocal. Hence, unlike the Hartree self-energy, which only yields a constant shift in the mass, the self-energy is now energy and momentum dependent and consists of several terms with different Dirac structure. Assuming a homogeneous medium with even parity, the inverse propagator can be parametrized as

$$S^{-1}(z,\vec{k}) = \gamma_0 z C(z,|\vec{k}|) - \vec{\gamma}\cdot\vec{k}A(z,|\vec{k}|) - B(z,|\vec{k}|), \qquad (20)$$

where z is a complex energy variable. In vacuum, as a consequence of Lorentz invariance, the dressing functions A, B, and C are only functions of $k^2 = z^2 - |\vec{k}|^2$, and the functions A and C are equal. In the medium, however, where we have a preferred frame, we have three independent functions, which depend on energy and momentum separately.

A. Model parameters and computational details

The integrals given in Sec. II are divergent and our model is only well-defined after specifying how to regularize them. Since the NJL model is nonrenormalizable, new cutoff parameters can appear at each loop order. For instance, even if we have regularized the quark loops in the

Hartree self-energy, Eq. (3), and the RPA polarization loop, Eq. (8), the loop over the meson momentum in $\Sigma^{(1)}$, Eq. (19), is in general still divergent and needs to be regularized separately.

In the following we regularize both, quark and meson loops, by sharp three-momentum cutoffs Λ and Λ_M, respectively. This has the advantage that it keeps the numerical effort for the involved self-consistency problem as simple as possible. Moreover, it preserves the analytic structure in the complex energy plane. The obvious disadvantage is that the three-momentum cutoffs violate the Lorentz covariance. For the moment, we take this as a minor problem, which could be improved on in future modifications of the model.

The noncovariance of the regularization also makes it necessary to specify how external three-momenta are distributed to the propagators in a loop. In the RPA polarization functions, Eq. (8), we distribute $\vec{q}$ equally to both quark propagators, whereas in the NLO meson loops, Eq. (19), we must attribute the entire external three-momentum to the quark propagator in order to be consistent with the derivation of this diagram from the Φ functional.

In addition to the cutoffs, the model has two more parameters, namely, the coupling constant and the bare quark mass. We take

$$\Lambda = 664.3 \text{ MeV}, \qquad G\Lambda^2 = 2.06, \qquad m_0 = 5.0 \text{ MeV}, \tag{21}$$

which in leading order (Hartree/RPA) yield the empirical vacuum values for the pion mass $m_\pi = 135.0$ MeV and pion decay constant $f_\pi = 92.4$ as well as a quark condensate of $\langle \bar{u}u \rangle^{1/3} = -250.8$ MeV [22]. This corresponds to a constituent mass $m_H = 300$ MeV. In principle, a refit of these parameters should be done at NLO. However, for the mostly explorative studies of the present paper, we keep them unchanged. The meson loop cutoff is set to $\Lambda_M = 500.0$ MeV.

The gap equation is solved iteratively starting with a Hartree-like ansatz for the quark propagator. The dressing functions are stored on a grid. In energy direction the grid is fixed through the Matsubara frequencies and in three-momentum direction an equidistant grid space of 50 MeV is chosen. Values in between the grid points are interpolated with cubic splines. The inverse propagators of the intermediate mesons are also stored on a grid.

B. Dressing functions and intermediate meson propagators

Results for the dressing functions A, B, and C are displayed in Fig. 6. To a good approximation they can be taken to represent the dressing functions in vacuum, although for numerical reasons they have been calculated at a temperature of 10 MeV and are therefore only given at discrete Matsubara frequencies. The results should be compared with the Hartree results, which are $B_H = m_H = 300$ MeV for the present parameters and $A_H = C_H = 1$. As one can see, the NLO corrections lead to an overall reduction of the B function, whereas A and C are slightly enhanced. All dressing functions have in common that they are maximal at the lowest $|\omega_n|$ and monotonously decrease with increasing $|\omega_n|$. (Note that the functions are symmet-

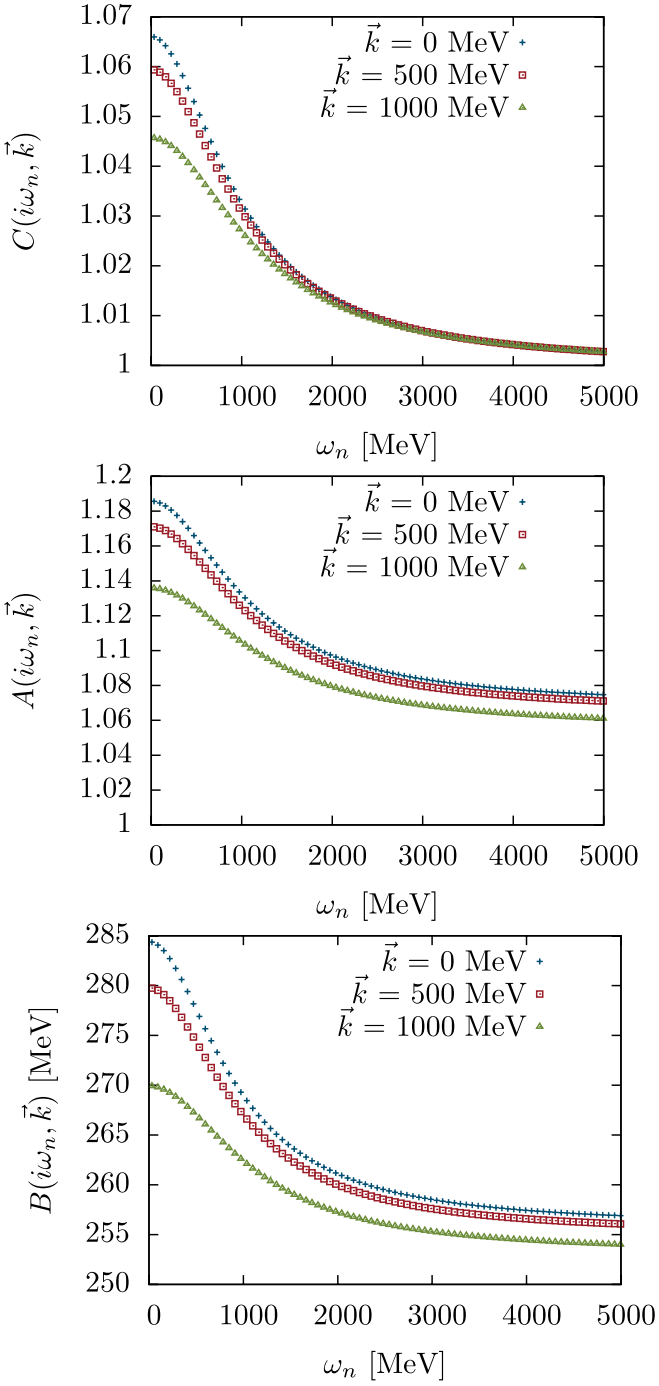

FIG. 6 (color online). Dressing functions C, A, and B of the quark propagator at $T = 10$ MeV and $\mu = 0$ as functions of the Matsubara frequency for different three-momenta.

ric in ω_n.) The same behavior can be observed with increasing three-momentum. Asymptotically, the NLO self-energy contribution vanishes, and the B function approaches a constant value coming from the Hartree diagram. For the same reason the C function converges to the trivial value of 1.

In principle, we would expect the same behavior for the A function. In fact, because of Lorentz covariance, the functions A and C should be equal in vacuum. However, as a consequence of the noncovariant regularization, this turns out not to be the case. Moreover, when we consider the nontrivial parts $A-1$ and $C-1$, the symmetry violation is of the same order of magnitude as the physical effect. A closer inspection reveals that the A function is most strongly affected by the cutoff artifacts, because it is directly related to the three-momentum [see Eq. (20)]. In particular, this explains the wrong asymptotic behavior of A. Hence, if we are interested in results which are sensitive to $A-1$, an improved regularization scheme should be employed. For the quark condensate, which we discuss in Sec. IV C, we expect that the situation is less problematic, as it is mainly influenced by the scalar function B [see Eqs. (23) and (24) below].

In Fig. 7 the intermediate RPA propagators in the pion (upper panel) and sigma (lower panel) channel at $T=10$ MeV and $\mu=0$ are displayed as functions of the Matsubara frequency for vanishing three-momentum. The numerical results are indicated by points. For comparison we also show the corresponding propagators in the Hartree + RPA scheme. As discussed at the end of Sec. III the latter are constrained by chiral Ward identities whereas the intermediate RPA propagators in the NLO scheme are not. In Fig. 7 this is reflected by the fact that the peak of the pion propagator at $\omega_m=0$ is strongly suppressed in the NLO scheme: In Hartree + RPA the peak is due to the relatively near-by pole at real energies, $q^0=m_\pi=135$ MeV. The strong reduction of this peak in NLO is thus a hint for a considerably larger mass of the intermediate pion.

We can estimate the meson masses by fitting the numerical points with a simple pole ansatz,

$$D_M(i\omega_M,\vec{0})\approx-\frac{Z_M}{\omega_m^2+m_M}-2G. \tag{22}$$

The constant $-2G$ has to be taken into account to get the correct asymptotic behavior [cf. Eq. (41) below]. These fits are indicated by the lines in Fig. 7. In Hartree + RPA we find $m_\pi\approx 137$ MeV, in good agreement with the true pole mass of 135 MeV. For the intermediate RPA pion in NLO, on the other hand, the fit yields $m_\pi\approx 340$ MeV.

In the sigma channel, the situation is less dramatic because the sigma meson is not a Goldstone boson. Here the pole fit yields $m_\sigma\approx 670$ MeV in Hartree + RPA and a slightly lower mass for the intermediate RPA sigma in NLO. However, these numbers should not be trusted too much, as they are based on rather far extrapolations from imaginary to real energies. (In fact, in the MEM analysis in the next section, we find masses which are 10%–15% lower.)

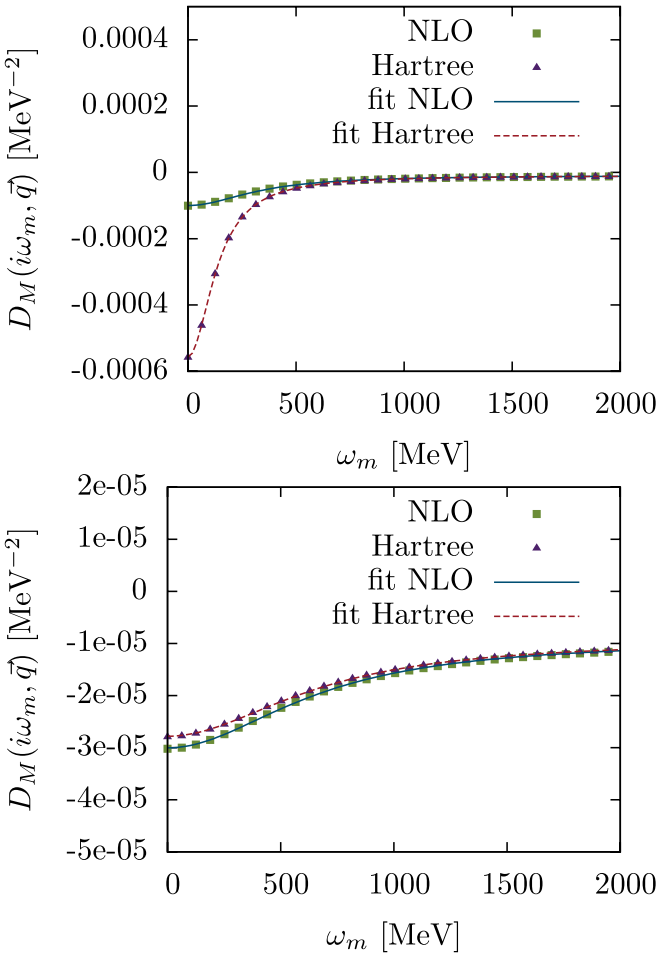

FIG. 7 (color online). Pion (upper panel) and sigma (lower panel) propagators at $T=10$ MeV and $\mu=0$ as functions of the Matsubara frequency for vanishing three-momentum. The intermediate RPA propagators based on the self-consistent solutions of the NLO gap equation are compared with the propagators in the Hartree + RPA scheme. The numerical results at the discrete Matsubara frequencies are indicated by points whereas the lines correspond to fits according to Eq. (20).

In Fig. 8 we show the behavior of the intermediate sigma and pion propagators in the chiral limit at the chiral restoration temperature, $T=T_c$. As chiral symmetry is restored, sigma and pion are now degenerate. However, even at T_c the intermediate RPA mesons do not become massless. Fitting again the numerical points with Eq. (22), we find $m_\pi=m_\sigma\approx 270$ MeV. This will be relevant for the discussion below.

C. The quark condensate

The chiral quark condensate is a scalar quantity and can be calculated directly in Euclidean (Matsubara) space,

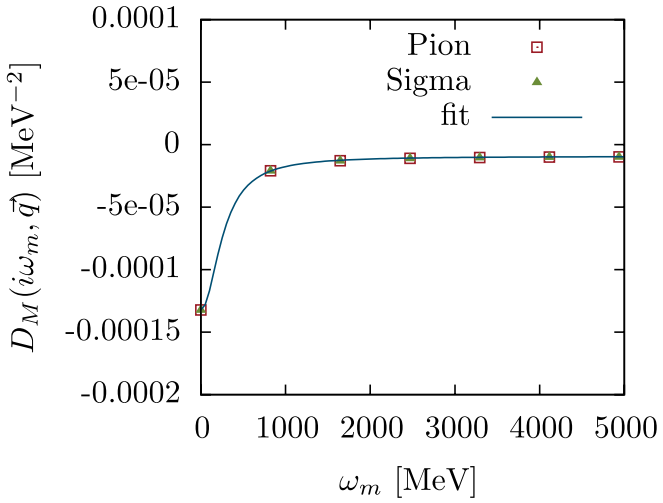

FIG. 8 (color online). Intermediate sigma and pion propagators in the NLO scheme in the chiral limit at $\mu = 0$ and $T = T_c = 131$ MeV as functions of the Matsubara frequency for vanishing three-momentum.

$$\langle \bar{q}q \rangle_T = T \sum_n \int \frac{d^3k}{(2\pi)^3} \mathrm{Tr}(S(i\omega_n, \vec{k})), \tag{23}$$

where

$$\mathrm{Tr}(S(i\omega_n, \vec{k})) = -8N_c \frac{B(i\omega n, \vec{k})}{\omega_n^2 C^2(i\omega n, \vec{k}) + \vec{k}^2 A^2(i\omega_n, \vec{k}) + B^2(i\omega_n, \vec{k})}, \tag{24}$$

cf. Eq. (20).

Our results for its temperature dependence in the chiral limit are displayed in Fig. 9, both, in Hartree approximation (dashed) and in NLO (solid). We find that chiral symmetry is restored in a second-order phase transition in both cases. The critical temperature is decreased by the NLO corrections.

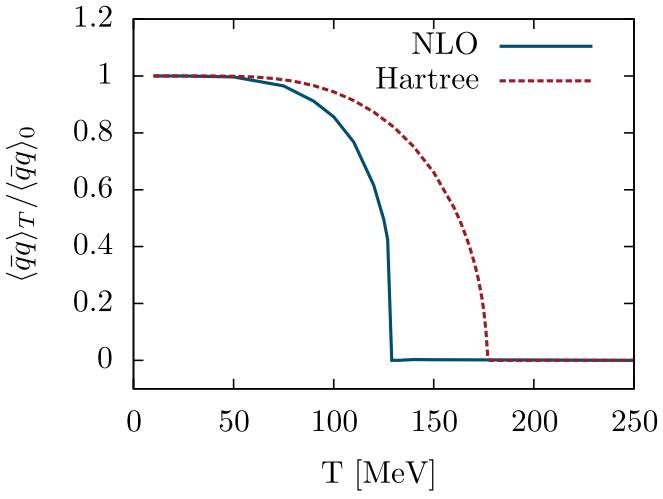

FIG. 9 (color online). Temperature dependence of the chiral quark condensate in the chiral limit in Hartree approximation (dashed) and in NLO (solid) at $\mu = 0$.

A second-order phase transition is also what is expected for two-flavor QCD in the chiral limit. At the critical temperature the fermionic degrees of freedom are suppressed due to their antiperiodicity. Therefore the phase transition is dominated by four bosonic degrees of freedom (three pions and the sigma meson) which are all massless at T_c and one expects critical behavior according to the $O(4)$ universality class [18]. Since these arguments are only based on the symmetries and dimensionality of the system, the same should hold in any theory or model with the same conditions. Indeed, a second-order phase transition with $O(4)$ critical exponents has been found in a renormalization group approach to the two-flavor quark meson model [23,24], and the NJL model should in principle exhibit a similar behavior.

However, it is not *a priori* clear to what extent the universal behavior is spoiled by the truncation scheme. As we have seen, the massless bosonic degrees of freedom which are the basis of the universality arguments are not manifest in the gap equation, neither in Hartree approximation nor in NLO: In the Hartree self-energy, there is no back-reaction of the RPA mesons on the quark propagator, whereas the intermediate RPA mesons which enter the NLO gap equation are not massless. From this point of view, it seems not even guaranteed that the phase transition must be second order in these approximation schemes. To understand why this nevertheless should be expected, we can adopt the arguments of Ref. [25], where the chiral phase transition was investigated in a purely bosonic model at NLO and found to be second order as well: As we have discussed, at each order one can in principle construct mesonic correlators with the correct chiral behavior by applying Eq. (15) to the Φ functional and iterating the resulting scattering kernel in the BSE. One could then employ these correlators to study critical exponents. Obviously, this can only work if the phase transition is second order. Thus, the gap equation must somehow "know" about the massless degrees of freedom even if they do not enter the equation explicitly.

In this context the consistency of the approximation scheme is crucial: In Refs. [13,15] a first-order phase transition was found in a simplified NLO scheme, which was suggested in Refs. [9,12]. In that scheme, only local contributions to the quark self-energy are taken into account. Although one can formally show that there are massless Goldstone bosons in the chiral limit, the approximation is not thermodynamically consistent as the gap equation cannot be derived from a thermodynamic potential. This suggests that a thermodynamically consistent treatment is important to find the correct order of the phase transition.

Yet, even in a self-consistent and thermodynamically consistent truncation scheme, not all details of the critical behavior are necessarily reproduced correctly. It is well known that the Hartree gap equation, although correctly predicting a second-order phase transition, yields mean-field critical exponents. At NLO, there might be some improvement, but we should not expect to find exact $O(4)$ behavior. Unfortunately, our numerical results are not precise enough to work this out quantitatively.

The low-temperature behavior of the quark condensate is model independently given by chiral perturbation theory. For two quark flavors one finds in the chiral limit [26]

$$\langle \bar{q}q \rangle_T = \langle \bar{q}q \rangle_0 \left(1 - \frac{T^2}{8 f_\pi^2} - \frac{T^4}{384 f_\pi^4} + \ldots \right), \qquad (25)$$

where $\langle \bar{q}q \rangle_0$ is the condensate at $T = 0$ and f_π is the pion decay constant. This behavior is entirely due to the massless chiral pions. The T^2 term corresponds to their ideal gas contribution, while the T^4 term is due to p-wave $\pi - \pi$ interactions.

Obviously, this behavior cannot be reproduced in the Hartree approximation, which includes no back-coupling of the mesons to the quark propagator. The change of the condensate is then exclusively triggered by thermal quarks and, hence, exponentially suppressed due to their mass.

On the other hand, it was shown in Ref. [15] that at least the T^2 term in Eq. (25) is reproduced correctly, if the $1/N_c$ corrections to the quark propagator are taken into account perturbatively. To be more precise, it was shown that the leading correction corresponds to that of an ideal gas of RPA pions. Since in the perturbative approach the latter are built from Hartree quarks, they are massless in the chiral limit and, thus, lead to the correct low-temperature behavior.

Accordingly, the T^2-term in Eq. (25) cannot be reproduced in our fully self-consistent NLO scheme. As in the perturbative approach, there are corrections from the intermediate RPA mesons. However, because of their relatively large masses, their effect is exponentially suppressed. We are thus faced with the situation that the self-consistent scheme gives only a poor description of the low-temperature behavior but works well at the phase transition, while it is just the other way around in the perturbative approach.

In Fig. 10 we show the temperature dependence of the quark condensate for the case of a nonvanishing bare quark mass. In this case, chiral symmetry is only approximately restored in a crossover. Again, the NLO corrections lead to a reduction of the crossover temperature relative to the Hartree result.

The dependence of the quark condensate on the chemical potential at $T = 0$ can be seen in Fig. 11 for the chiral limit. The Hartree and NLO results look qualitatively similar. In both cases chiral symmetry is restored in a first-order phase transition. Similar to the temperature behavior, the critical chemical potential is slightly lower in NLO.

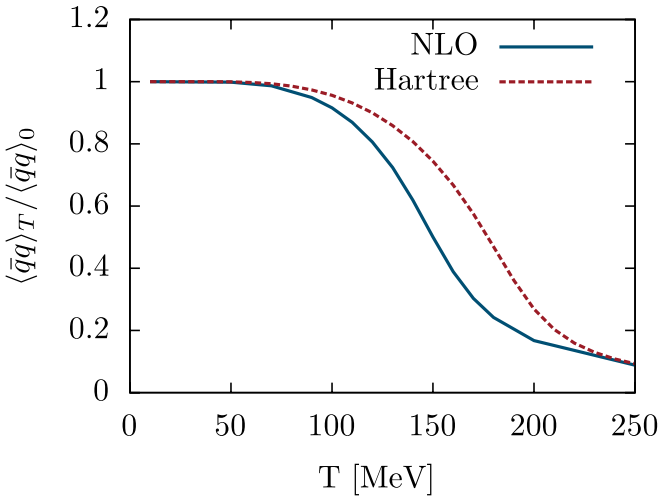

FIG. 10 (color online). Temperature dependence of the quark condensate for a bare quark mass $m_0 = 5$ MeV in Hartree approximation (dashed) and NLO (solid) at $\mu = 0$.

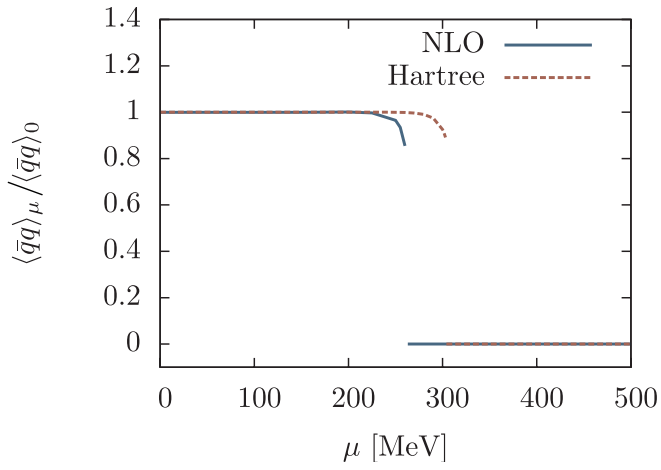

FIG. 11 (color online). Quark condensate in the chiral limit as a function of the chemical potential in Hartree approximation (dashed) and NLO (solid) at $T = 0$.

V. ANALYTIC CONTINUATION WITH THE MAXIMUM-ENTROPY METHOD (MEM)

Searching the analytic continuation of a propagator given at a discrete set of Matsubara frequencies is an ill-posed problem. In general, an infinite set of functions would provide an analytic continuation. Additional requirements on asymptotics and analytical structure provide a unique solution [27] but this only helps if one can get analytic expressions for the functions.

One way to attack this problem numerically is the maximum-entropy method. The quantity to calculate is the spectral function $\rho(\omega)$ which is related to the propa-

gator via the Lehmann representation (e.g. [28]),

$$D(z) = \int_{-\infty}^{\infty} \frac{d\omega}{2\pi} \frac{\rho(\omega)}{z - \omega}, \tag{26}$$

and can be interpreted as a probability distribution. The method performs a χ^2 fit to the discrete "data" $D(i\omega_n)$ and additionally requires minimum deviation from the so-called prior estimate, the "most probable" spectral function in absence of any data. The combination of both requirements finally leads to a unique solution. MEM has been successfully used in lattice QCD [29,30] and Dyson-Schwinger calculations [31].

A. The Method

We largely follow the formalism described in Refs. [29,31]. The basis for MEM is Bayes' theorem for conditioned probability applied to the plausibility $P[\rho|DH(m)]$ of a spectral function ρ under given data D and a prior knowledge $H(m)$,

$$P[\rho|DH(m)] = \frac{P[D|\rho H(m)]P[\rho|H(m)]}{P[D|H(m)]}. \tag{27}$$

$P[D|\rho H(m)]$ is the likelihood function, which indicates the plausibility of the data under the spectral function and the prior and $P[\rho|H(m)]$ is the prior probability for the plausibility of ρ solely under the prior. $P[D|H(m)]$ is a normalization factor independent of the spectral function and can be dropped as the probabilities are normalized in the end.

For the likelihood function a Gaussian distribution is assumed

$$P[D|\rho H(m)] = \frac{1}{Z_L} e^{-L[\rho]} \tag{28}$$

with

$$L[\rho] = \frac{1}{N_D} \sum_i \frac{|D_i - D_i^\rho|^2}{2|\sigma_i|^2} \tag{29}$$

for N_D equidistant "data" with values D_i and errors σ_i and the corresponding values D_i^ρ calculated from the given spectral function ρ using the Lehmann representation, Eq. (26). Z_L is a normalization constant. Note that, by this assumption, $P[D|\rho H(m)]$ does actually not depend on the prior.

The prior probability $P[\rho|H(m)]$ depends directly on a prior estimate $m(\omega)$ for the spectral function. $m(\omega)$ contains general information about spectral functions, especially positivity, and is usually chosen as a constant function. With help of a scale factor α, $P[\rho|H(m)]$ can be expressed as

$$P[\rho|H(m)] = \int_0^\infty d\alpha P[\rho|H(\alpha m)]P[\alpha|H(m)], \tag{30}$$

where

$$P[\rho|H(\alpha m)] = \frac{1}{Z_S} e^{\alpha S[\rho]} \tag{31}$$

with a normalization constant Z_S and the Shannon-Jaynes entropy

$$S[\rho] = \int_{-\infty}^{\infty} d\omega \left(\rho(\omega) - m(\omega) - \rho(\omega) \ln \frac{\rho(\omega)}{m(\omega)}\right). \tag{32}$$

This can be derived axiomatically by using general features of the entropy (locality, scale invariance, etc.) or with help of the law of large numbers ("monkey argument") [29]. Discretization and expanding the logarithm for small deviations of the spectral function from the prior yields

$$S[\rho] \approx -2 \sum_i \Delta\omega_i (\sqrt{\rho_i} - \sqrt{m_i})^2. \tag{33}$$

Applying Eq. (28) and (31) to Eq. (27) gives

$$P[\rho|DH(\alpha m)] = \frac{1}{Z} e^{Q[\rho]} \tag{34}$$

with another normalization constant Z and the functional $Q[\rho] = \alpha S[\rho] - L[\rho]$. Maximizing $Q[\rho]$ gives the most probable spectral function, $\rho(\omega) = \rho_\alpha(\omega)$, for given α.

Finally the scale factor α has to be eliminated, which can be done in several ways. We use Bryan's method [32], which is applied in most cases. Here, the final spectral function $\rho_{\mathrm{MEM}}(\omega)$ is obtained by averaging over α,

$$\begin{aligned} \rho_{\mathrm{MEM}}(\omega) &= \int D\rho \rho(\omega) P[\rho|DH(m)] \\ &\approx \int_0^\infty d\alpha \rho_\alpha(\omega) P[\alpha|DH(m)], \end{aligned} \tag{35}$$

with the probability factor

$$\begin{aligned} P[\alpha|DH(m)] &\propto \int D\rho e^{Q[\rho]} \\ &\approx \exp\left[\frac{1}{2} \sum_k \ln\left(\frac{\alpha \Delta\omega k}{\lambda_k}\right) + Q[\rho_\alpha]\right]. \end{aligned} \tag{36}$$

and λ_k being the eigenvalues of the matrix

$$M_{ij} = \alpha \Delta\omega_i \delta_{ij} + \sqrt{\rho_i} \frac{\partial^2 L}{\partial\rho_i \partial\rho_j} \sqrt{\rho_j}|_{\rho=\rho_\alpha} \tag{37}$$

In an intermediate step Laplace's rule ($P[\alpha|H(m)] =$ const.) [29] has been applied. For calculating $\rho_{\mathrm{MEM}}(\omega)$ the probabilities Eq. (36) have to be normalized.

B. Numerical implementation

The iterative calculation of the quark propagator discussed in Sec. IV has been performed without error estimate, as the largest parts of the error are highly correlated and systematical. MEM requires data with noncorrelated Gaussian errors [Eq. (29)]. Therefore we assume a constant relative error of 10^{-4} all data points. This error underestimates the systematical errors but should be of the order

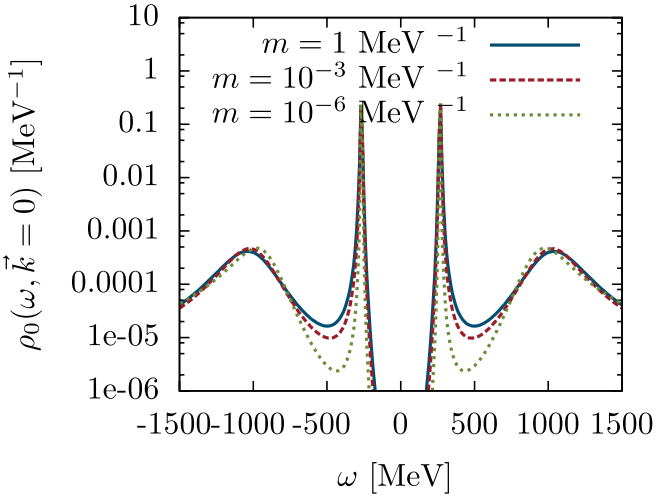

FIG. 12 (color online). MEM result for the NLO quark spectral function $\rho_0(\omega)$ in vacuum for vanishing three-momentum, using different priors $m(\omega) = \text{const}$.

the uncorrelated numerical errors. This choice seems useful as larger errors do not resolve the continuum contributions to the spectral functions while smaller errors lead to unphysical oscillations.

We chose a constant prior of $m(\omega) = 10^{-3}$ MeV^{-1}. This arbitrary choice can be justified as the result is quite insensitive, even when the prior is varied by 6 orders of magnitude, as illustrated in Fig. 12.

C. Vacuum spectral functions

Vacuum[2] results for the quark spectral function are shown in Fig. 13. To be precise, since the spectral function of spin-$\frac{1}{2}$ fermions has a Dirac structure, we show the 0-component,

$$\rho_0 = \tfrac{1}{4}\mathrm{Tr}(\gamma^0 \rho). \tag{38}$$

Moreover, we consider quarks with vanishing three-momentum.

The Hartree spectral function is displayed in the upper panel. Here we can directly compare the MEM result with the exact analytical solution,

$$\rho_0(\omega) = \pi\delta(|\omega| - m_H), \tag{39}$$

i.e., two delta peaks at $\omega = \pm 300$ MeV. Indeed, MEM yields two sharp peaks at the correct positions, although with a small width which is caused by the assumed numerical errors.

[2]As before, the "vacuum" results have been obtained at $\mu = 0$ and a temperature $T = 10$ MeV for numerical reasons. We expect the difference to real vacuum calculations at $T = 0$ to be small.

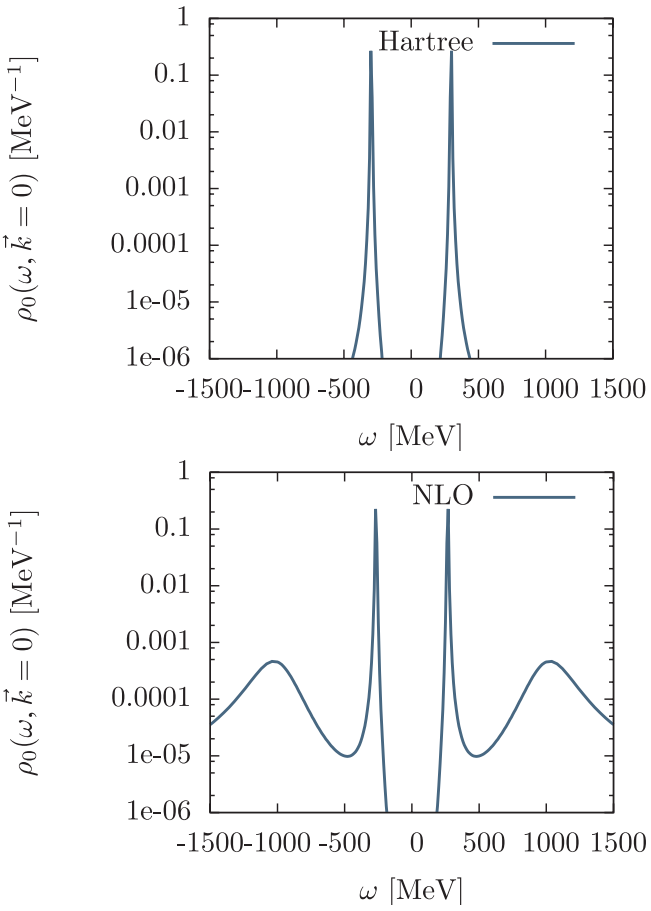

FIG. 13 (color online). MEM results for the quark spectral function $\rho_0(\omega)$ in Hartree approximation (upper panel) and NLO (lower panel) in vacuum for vanishing three-momentum.

The NLO spectral function (lower panel) has similar peaks, shifted to slightly lower energies, $\omega \approx \pm 270$ MeV. In addition there are two broad bumps at higher values of $|\omega|$. These structures can be related to the imaginary part of the NLO self-energy diagram (last diagram of Fig. 5), i.e., to the continuum due to meson absorption or emission processes on the quark. This continuum should be well separated from the quark mass peak and start at a threshold given by the sum of the quark mass and the intermediate pion mass. According to our earlier estimate for m_π, this would be at around 600 MeV and is more or less consistent with the MEM result. The details of the threshold region can, however, not be resolved. From Fig. 12 we also see that the dip region, where we expect a vanishing spectral function, is most sensitive to the prior.

Unlike in Hartree approximation, the MEM results for the spectral functions in the self-consistent NLO scheme cannot be confronted with direct calculations in Minkowski space, since the latter are highly nontrivial. However, such a comparison can be done for the quark propagator with *perturbative* NLO corrections to the self-energy. In that case, as already mentioned, only the Hartree

propagator S_H is calculated self-consistently and afterwards perturbative corrections are added to the self-energy,

$$S_{\text{pert}}^{-1} = S_H^{-1} - \Sigma_{\text{pert}}^{(1)}, \tag{40}$$

where $\Sigma_{\text{pert}}^{(1)}$ is strictly of the order $1/N_c$. In particular, it is entirely given in terms of S_H and meson propagators in the Hartree + RPA scheme. This makes its evaluation in Minkowski space possible.

As discussed, e.g., in Ref. [15], $\Sigma_{\text{pert}}^{(1)}$ consists of two diagrams. The first one is local and, thus, only gives a constant real contribution to the mass. In the following comparison we will therefore neglect this term for simplicity. The second contribution is nonlocal and given by self-energy in the last diagram in Fig. 5 if all self-consistent quark propagators are replaced by S_H. In Minkowski space we make the additional approximation of neglecting the continuum parts and finite widths of the mass peaks of the RPA mesons. As the mass peaks are the dominant contributions to the spectrum and even for the unstable sigma meson the main peak is very sharp, this approximation should be quite accurate.

A comparison with the MEM output of a corresponding perturbatively dressed propagator calculated in Euclidean space is shown in Fig. 14. For numerical reasons the calculation in Minkowski space has been performed with quark propagators with a width of 1 MeV, which was added by hand. The main peak of the MEM result and the Minkowski result are almost at the same energy. (The small difference could be due to the mentioned approximations for the meson spectral function in Minkowski space.) The continuum contributions only show rough agreement in height and position but the shape differs considerably. The main reason for this is the dominance of the mass peak in the spectrum. The continua give only small contributions and it would require data with much lower errors to become sensitive to the shape of the continuum. Furthermore the continuum structure is very complicated with sharp thresholds and peaks which are difficult to be reproduced by MEM. In fact, the high-energy thresholds and peaks are artifacts of the regularization and therefore not even physical. In principle, one could try to include these effects into the prior $m(\omega)$ as done in the lattice calculations of Ref. [33].

For applying MEM to meson propagators we use a subtracted dispersion relation,

$$D_M(z) = \int_{-\infty}^{\infty} \frac{d\omega}{2\pi} \frac{\rho(\omega)}{z - \omega} - 2G, \tag{41}$$

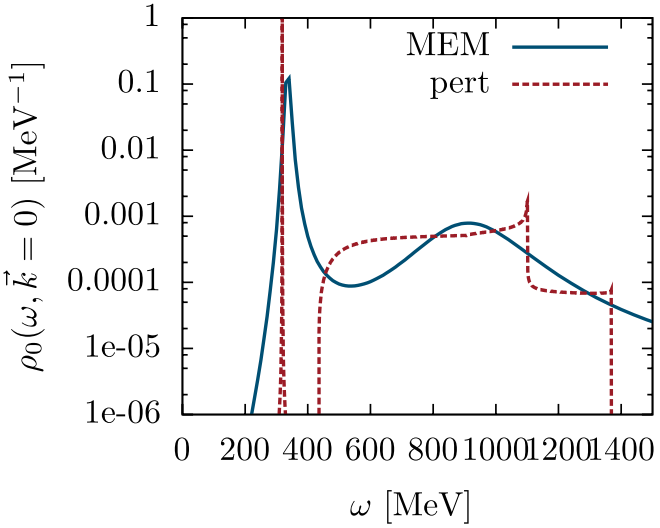

FIG. 14 (color online). Comparison between MEM result and direct Minkowski-space calculation of the quark spectral function with perturbative $1/N_c$ corrections to the self-energy in vacuum.

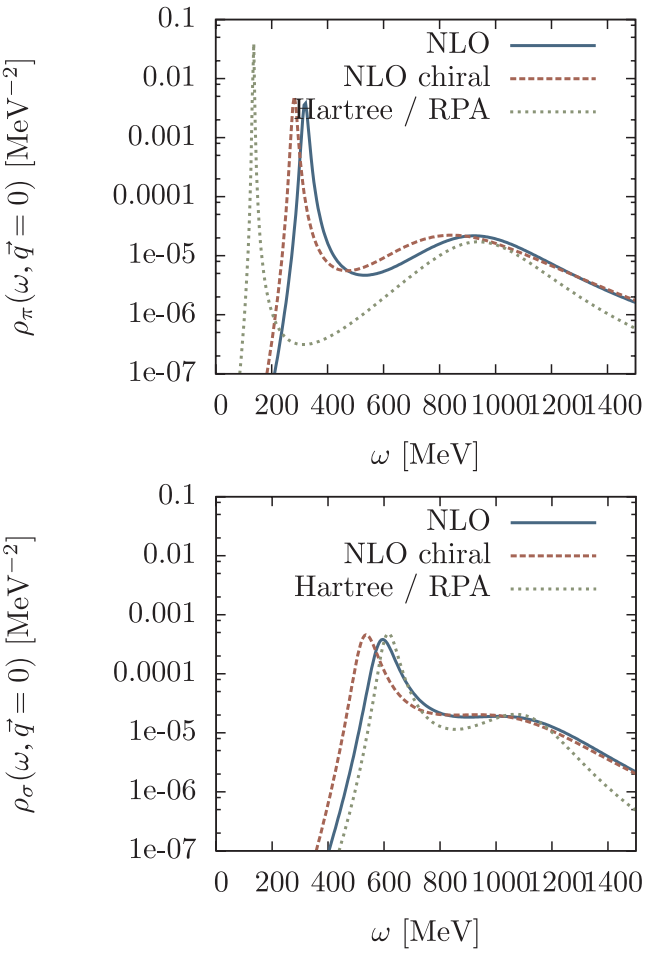

FIG. 15 (color online). MEM results for the RPA pion (upper panel) and sigma (lower panel) spectral function in vacuum for vanishing three-momentum. The various curves correspond to the intermediate RPA mesons in the NLO scheme for $m_0 = 5$ MeV and in the chiral limit, as well as in the Hartree + RPA scheme for $m_0 = 5$ MeV.

which takes care of the asymptotic behavior of NJL RPA meson propagators.

The spectral functions for the RPA meson propagators are displayed in Fig. 15. The intermediate RPA mesons in the NLO scheme with finite current quark mass and in the chiral limit are compared with the mesons in the Hartree + RPA scheme.

The latter can also be calculated directly in Minkowski space (cf. Sec. V D). In the pion channel this yields a delta peak at $\omega = m_\pi = 135$ MeV and a continuum due to quark-antiquark decay above a threshold of $2m_H = 600$ MeV. As one can see in the figure (upper panel, dotted line), these features are again qualitatively reproduced by MEM: We find a sharp peak at 135 MeV and a broad bump at higher energies, which can be identified with the continuum. On the other hand, as before, the detailed threshold behavior cannot be reproduced.

The spectral function of the intermediate RPA pion in NLO (solid line) looks qualitatively similar, but the mass peak is now located at $\omega = 320$ MeV. This is slightly lower than our estimate by the pole fit in Sec. IV B (340 MeV), but still very heavy. As we have said repeatedly, this reflects the fact that the intermediate RPA mesons are not constrained by chiral Ward identities. In fact, even in the chiral limit (dashed line), we find a mass peak at 280 MeV in the MEM spectral function.

In the sigma channel, the exact spectral function in Hartree + RPA has a mass peak slightly above the continuum threshold. This is again qualitatively reproduced by MEM (lower panel, dotted line), where we find a maximum at about 615 MeV. The NLO corrections to the sigma are rather small (solid line), the mass is lowered by about 20 MeV. In the chiral limit (dashed line), it is further reduced by 60 MeV, but the gross features of the spectral function remain unchanged.

D. In-medium spectral functions

Larger temperatures increase the inaccuracies significantly as the larger distance between the Matsubara frequencies ($2\pi T$) provides only few data at low frequencies while high-frequency data mainly carry information about the asymptotics.

As for larger temperature the quark mass decreases and therefore the main peaks in the spectral function come closer together, extrapolating the 0-component of the spectral function with MEM does not resolve the single peaks. Therefore it is reasonable to study other projections of the spectral function to separate the peaks. For vanishing three-momentum this can be achieved by the decomposition of the spectral function

$$\rho(\omega) = \rho^+(\omega) L^+ \gamma_0 + \rho^-(\omega) L^- \gamma_0 \tag{42}$$

with the projectors $L^\pm = \frac{1}{2}(1 \pm \gamma_0)$. The components $\rho^\pm$ correspond to the spectra of particle and antiparticles and are also positive definite, therefore MEM is applicable. In Hartree approximation the analytic result yields

$$\rho^+(\omega) = \pi\left(1 + \frac{m}{\omega}\right)\delta(\omega - m) \tag{43}$$

$$\rho^-(\omega) = \pi\left(1 - \frac{m}{\omega}\right)\delta(\omega + m) \tag{44}$$

and the two main peaks are separated into the different channels. This decomposition has also been used in recent lattice studies at finite temperature [34].

MEM results for $T = 200$ MeV are shown in Fig. 16. While in Hartree approximation the quark and antiquark peaks are still well-separated the NLO peaks are much broader and overlap. This is an indicator for the thermal broadening of the quark spectral function in the medium.

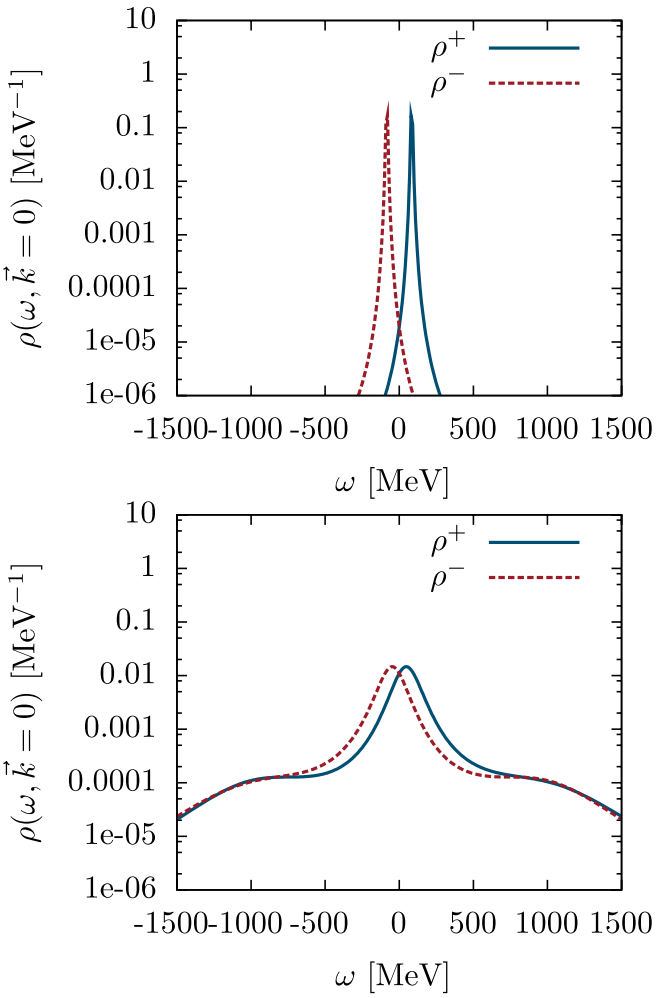

FIG. 16 (color online). MEM result for the quark spectral functions $\rho(\omega)$ in Hartree approximation (upper panel) and NLO (lower panel) for vanishing three-momentum at $T = 200$ MeV and $\mu = 0$. The solid (dashed) lines correspond to an assumed relative numerical error of 10^{-4} (10^{-6}).

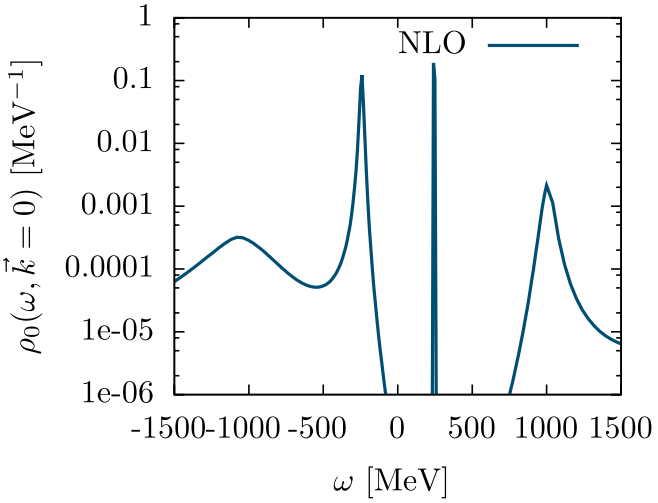

FIG. 17 (color online). MEM result for the NLO quark spectral function $\rho_0(\omega)$ for vanishing three-momentum at $T = 0$ and $\mu = 200$ MeV.

Applying MEM at finite chemical potential visualizes the shifted Fermi surface. The quark spectral function at $\mu = 200$ MeV is displayed in Fig. 17. We obtain a quite asymmetric result: At positive energies we find a very sharp mass peak which is well separated from the continuum at higher energies. At negative energies, on the other hand, both the mass peak and the continuum are broader and the dip region in between is less pronounced.

Although at finite chemical potential the spectral function is indeed in general no longer symmetric, the main reason for the observed asymmetry is probably caused by the MEM procedure. This is due to the fact that the dispersion relation is now of the form

$$S(i\omega_n + \mu) = \int_{-\infty}^{\infty} \frac{d\omega}{2\pi} \frac{\rho(\omega)}{i\omega_n + \mu - \omega}. \qquad (45)$$

Therefore, the integral is most sensitive to details of the spectral function near the Fermi surface, where it gives the largest contribution. Hence, in the present example, the MEM procedure works best around $\omega = 200$ MeV, which explains why the positive mass peak is much better resolved.

In the mesonic sector, Hartree + RPA meson spectral functions can be calculated directly in Minkowski space without further assumptions. A comparison with MEM results in the pion channel at $T = 100$ MeV is displayed in Fig. 18 for $|\vec{q}| = 0$ (upper panel) and 100 MeV (lower panel). In the Minkowski-space calculations, a width of 1 MeV was again added by hand to the propagators for numerical reasons.

We find that the agreement of the MEM results with the direct calculations is rather poor. Only the position of the main peak fits while the shape of the spectral function looks totally different. The spacelike particle-hole branch

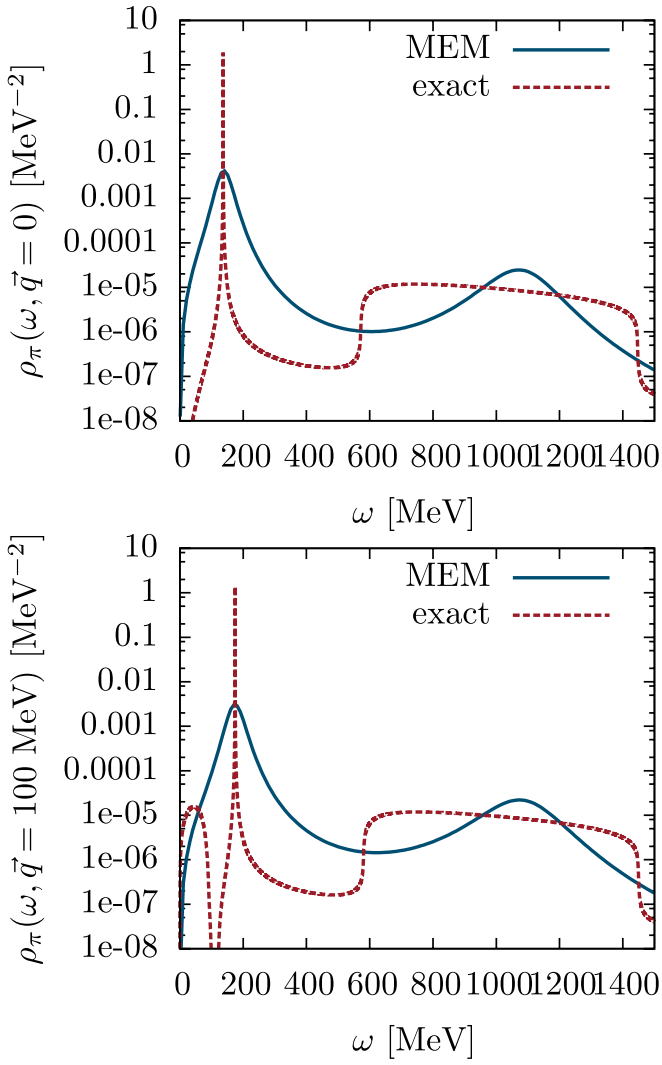

FIG. 18 (color online). Hartree + RPA pion spectral function in directly calculated in Minkowski space and extrapolated with MEM at $T = 100$ MeV for three-momentum $|\vec{q}| = 0$ (upper panel) and $|\vec{q}| = 100$ MeV (lower panel).

in the spectrum which occurs at finite three-momentum cannot be resolved in the MEM output.

In order to shed some light on this problem, we show in Fig. 19 the Euclidean data which served as input for the MEM results in Fig. 18. At low Matsubara frequencies the data points with different three-momenta are slightly shifted against each other, which takes care of the different mass peak positions. But one cannot see a qualitative difference which could produce the spacelike continuum contributions which exist at $|\vec{q}| = 100$ MeV, but not at $|\vec{q}| = 0$. Furthermore the complicated structure of the spectral functions is not visible in the Euclidean data and so this structure gets almost lost in the convolution with the Lehmann representation Eq. (26). Instead the fit of a propagator with a single mass pole according to a delta peak in the spectrum already fits the data almost perfectly.

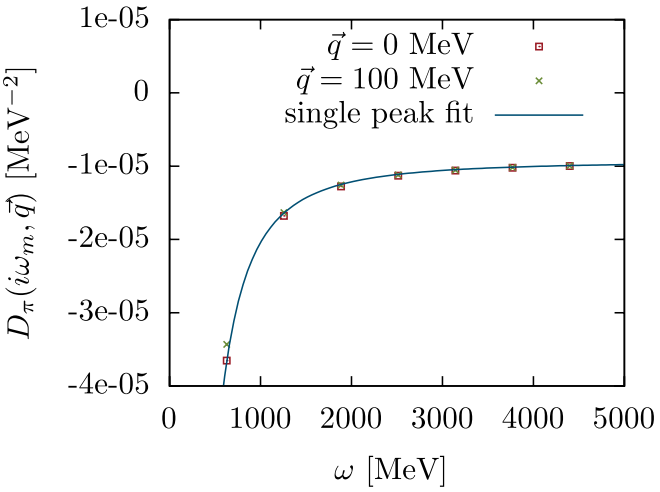

FIG. 19 (color online). Hartree + RPA Pion propagator in Euclidean space at $T = 100$ MeV. The line is the data coming from a spectral function with a single delta peak.

This exemplifies how difficult it is to regain the spectral function from the Euclidean data.

VI. SUMMARY

We have studied the NJL model in next-to-leading order in a self-consistent $1/N_c$ expansion. The chiral condensate shows a second-order phase transition at finite temperature and vanishing chemical potential in agreement with expectations from the $O(4)$ universality class. In comparison to mean-field results the critical temperature is decreased. The low-temperature behavior expected from chiral perturbation theory cannot be reproduced as the intermediate mesons which enter the NLO quark self-energy diagram are not restricted in terms of chiral symmetry and are very massive. At finite chemical potential and vanishing temperature the phase transition is of first order like in mean-field approximation. The critical chemical potential is also slightly reduced.

The maximum-entropy method has been used to calculate spectral functions for real energies from the Euclidean propagators. The mass peak of the particles can be reproduced quite well and for NLO quark propagators also a continuum contribution can be identified. The large mass of the intermediate pions is confirmed and approximately of order $\sim$320 MeV while the masses of the quarks (~ 270 MeV) and intermediate sigma mesons (~ 600 MeV) are of the order of the mean-field values. Finite temperature increases the inaccuracies of MEM as fewer data at low energies are available. For perturbatively dressed propagators the spectral function can be calculated directly in Minkowski space. A comparison with these results shows that the main peak is reproduced well by MEM, but not the continua.

ACKNOWLEDGMENTS

We thank Jürgen Berges, Bengt Friman, Hendrik van Hees, Jörn Knoll, and Andrey Radzhabov for useful discussions and comments about chiral symmetry and universality, and Dominik Nickel for his help with the maximum entropy method. D. M. was supported by BMBF under contract 06DA9047I and by the Helmholtz Graduate School for Hadron and Ion Research. We also acknowledge support by the Helmholtz Alliance EMMI and the Helmholtz International Center for FAIR.

[1] Y. Nambu and G. Jona-Lasinio, Phys. Rev. **122**, 345 (1961); **124**, 246 (1961).
[2] S. Hands and D. N. Walters, Phys. Lett. B **548**, 196 (2002).
[3] U. Vogl and W. Weise, Prog. Part. Nucl. Phys. **27**, 195 (1991).
[4] S. P. Klevansky, Rev. Mod. Phys. **64**, 649 (1992).
[5] T. Hatsuda and T. Kunihiro, Phys. Rep. **247**, 221 (1994).
[6] M. Iwasaki, H. Ohnishi, and T. Fukutome, arXiv:hep-ph/0606192.
[7] E. Quack and S. P. Klevansky, Phys. Rev. C **49**, 3283 (1994).
[8] D. Ebert, M. Nagy, and M. K. Volkov, Phys. At. Nucl. **59**, 140 (1996); Yad. Fiz. **59**, 149 (1996).
[9] V. Dmitrasinovic, H. J. Schulze, R. Tegen, and R. H. Lemmer, Ann. Phys. (Leipzig) **238**, 332 (1995).
[10] P. Zhuang, Phys. Rev. C **51**, 2256 (1995).
[11] D. Blaschke, Yu. L. Kalinovsky, G. Roepke, S. M. Schmidt, and M. K. Volkov, Phys. Rev. C **53**, 2394 (1996).
[12] E. N. Nikolov, W. Broniowski, C. V. Christov, G. Ripka, and K. Goeke, Nucl. Phys. **A608**, 411 (1996).
[13] W. Florkowski and W. Broniowski, Phys. Lett. B **386**, 62 (1996).
[14] M. Oertel, M. Buballa, and J. Wambach, Nucl. Phys. **A676**, 247 (2000).
[15] M. Oertel, M. Buballa, and J. Wambach, Phys. At. Nucl. **64**, 698 (2001); Yad. Fiz. **64**, 757 (2001); M. Oertel, Ph.D. thesis, TU Darmstadt, 2000.
[16] D. Blaschke, M. Buballa, A. E. Radzhabov, and M. K. Volkov, Yad. Fiz. **71**, 2012 (2008); Phys. At. Nucl. **71**, 1981 (2008).
[17] M. Kitazawa, T. Kunihiro, and Y. Nemoto, Phys. Lett. B **633**, 269 (2006).
[18] R. D. Pisarski and F. Wilczek, Phys. Rev. D **29**, 338 (1984).
[19] J. M. Luttinger and J. C. Ward, Phys. Rev. **118**, 1417 (1960).
[20] G. Baym and L. P. Kadanoff, Phys. Rev. **124**, 287 (1961).

[21] J. M. Cornwall, R. Jackiw, and E. Tomboulis, Phys. Rev. D **10**, 2428 (1974).
[22] M. Buballa, Phys. Rep. **407**, 205 (2005).
[23] B. J. Schaefer and J. Wambach, Phys. Rev. D **75**, 085015 (2007).
[24] B. J. Schaefer and H. J. Pirner, Nucl. Phys. **A660**, 439 (1999).
[25] M. Alford, J. Berges, and J. M. Cheyne, Phys. Rev. D **70**, 125002 (2004).
[26] J. Gasser and H. Leutwyler, Phys. Lett. B **184**, 83 (1987).
[27] G. Baym and N. D. Mermin, J. Math. Phys. (N.Y.) **2**, 232 (1961).
[28] M. Le Bellac, *Thermal Field Theory* (Cambridge University Press, Cambridge, 2000).
[29] M. Asakawa, T. Hatsuda, and Y. Nakahara, Prog. Part. Nucl. Phys. **46**, 459 (2001).
[30] I. Wetzorke, F. Karsch, E. Laermann, P. Petreczky, and S. Stickan, Nucl. Phys. B, Proc. Suppl. **106**, 510 (2002).
[31] D. Nickel, Ann. Phys. (Leipzig) **322**, 1949 (2007).
[32] R. K. Bryan, Eur. Biophys. J. **18**, 165 (1990).
[33] H. T. Ding, O. Kaczmarek, F. Karsch, H. Satz, and W. Söldner, arXiv:0910.3098.
[34] F. Karsch and M. Kitazawa, Phys. Rev. D **80**, 056001 (2009).